# Wide-angle wavelength-selective multilayer optical metasurfaces robust to interlayer misalignment

**Ping-Chun Li and Edward T. Yu***

*Microelectronics Research Center, University of Texas at Austin, 10100 Burnet Rd., Austin, Texas 78758, USA*
**Corresponding author: ety@ece.utexas.edu*

Received August 23, 2012; revised November 6, 2012; accepted November 6, 2012;
posted November 7, 2012 (Doc. ID 174843); published December 4, 2012

Multilayer plasmonic optical metasurfaces are demonstrated and analyzed that provide highly wavelength-selective reflectance that is robust to variation in angle of incidence and highly tolerant of misalignment of features between vertically stacked layers. Structures containing two layers of Ag nanostructure arrays separated by a dielectric layer are shown to provide reflectance >75% and transmittance <1% over a bandwidth of ~100 nm, with minimal variation for angles of incidence varying from 0° to 30°. These characteristics are shown to be robust to variations in vertical alignment between layers comparable to the array period. An analysis of these characteristics in terms of plasmonic behavior of individual Ag nanostructures, interference effects between multiple layers of nanostructure arrays, and phase shifts produced at each array layer is presented. 

*OCIS codes:* 330.1690, 050.6624.

## 1. INTRODUCTION

Plasmonic resonances in metal nanostructures have been widely exploited for a broad range of applications, including chiral metamaterials [1], nanoantennas [2], surface-enhanced Raman spectroscopy [3], biosensing [4], absorbers [5–7], and metamagnetism [8]. While such behavior can often be observed in structures fabricated in primarily planar geometries, there has been increasing interest in three-dimensional plasmonic nanostructures for applications including three-dimensional optical metamaterials with negative refractive index [9] and sensing or spectroscopy of biological molecules [10,11]. In addition, the role of phase in understanding and controlling light propagation via scattering from plasmonic nanostructures is of increasing interest [12,13]. Many such concepts rely upon the high sensitivity of plasmonic resonances in metal nanostructures to variations in size, spacing, and local dielectric environment. From a manufacturing perspective, however, it would be highly desirable to be able to engineer properties based on plasmonic resonances that are robust to variations in the precise dimensions of the constituent nanostructures.

In this paper, we report the design, experimental demonstration, and analysis of structures consisting of multiple layers of two-dimensional plasmonic arrays, with each individual layer constituting a subwavelength-scale metasurface [14,15]. These structures are shown to provide high reflectivity and low transmittance at optical wavelengths across a bandwidth of ~100 nm that remains fixed under variations in angle of incidence from 0° to 30°. In this respect, these structures provide new functionality compared to analogous, more conventional optical components such as dichroic mirrors, which provide high reflectivity over a specific range of wavelengths but are highly sensitive to variations in angle of incidence [16]. Designs are demonstrated that provide either polarization-independent or polarization-sensitive optical behavior, as well as robustness to large variations in vertical alignment between metasurface layers. These behaviors are shown to be a consequence of plasmonic resonances in metal nanostructures that constitute the individual metasurface layers, interference effects between metasurface layers, scattering phase shifts at each metasurface, and the interplay among these phenomena.

## 2. EXPERIMENT

Figure 1 shows schematic diagrams and scanning electron micrographs of the multilayer metasurface structures employed in these studies, along with the measurement geometries for transverse electric (TE) and transverse magnetic (TM) polarizations. All structures were fabricated on 0.5 mm thick glass substrates (CoreSix) polished to yield a surface roughness of 0.5 nm. Each metasurface layer consists of Ag nanostructure arrays created via electron beam lithography followed by deposition of 2 nm Ge/30 nm Ag using e-beam evaporation and, finally, a standard liftoff process. The individual Ag elements consist of 30 nm high square patches of side length $W$, and for each metasurface layer these are arranged in a square array of period $L$. Between individual metasurface layers, the sample structure is planarized using a spin-on glass whose thickness, $D$, is controlled via dilution of the spin-on-glass solution and spin-coating speed. For a structure containing two metasurface layers with structure (side length and array period) given by $W_1$, $L_1$ and $W_2$, $L_2$, respectively, the alignment between the individual metasurfaces is characterized by $S_x$, and $S_y$, as indicated in Fig. 1. Since the periods of each metasurface layer are related by a rational multiple $N/M$, i.e., $NL_1 = ML_2$, we define the translational offsets in the plane of the metasurface, $S_x$, and $S_y$, to be the minimum distances in the $x$- and $y$-directions, respectively, that one metasurface layer would have to be shifted such that the centers of individual array elements spaced by $NL_1 = ML_2$ are perfectly aligned.

Optical transmittance measurements were performed using collimated light from a halogen lamp spectrally resolved by

 

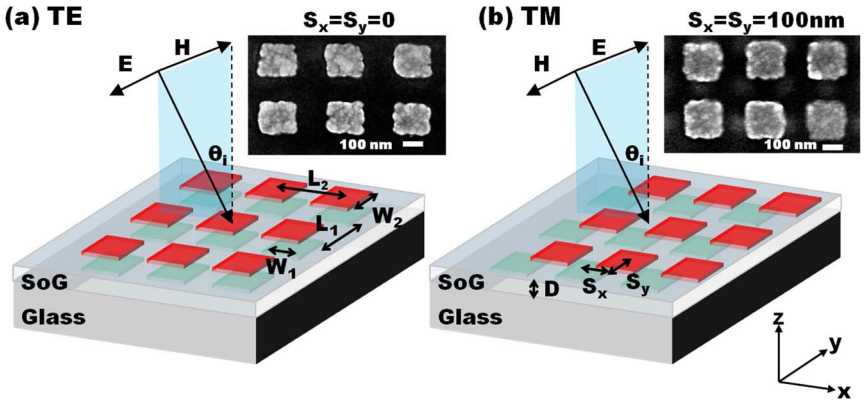


Fig. 1. (Color online) Schematic diagram of the multilayer metasurface structure on a glass substrate under (a) TE and (b) TM polarized illumination. $L_1$, $W_1$ and $L_2$, $W_2$ indicate the periodicity of the array and size of the individual metallic nanostructures for the bottom and top metasurface layers, respectively. The translational alignment parameters $S_x$ and $S_y$ are indicated in (b). The insets show the scanning electron micrographs of an aligned ($S_x = S_y = 0$), and shifted ($S_x = S_y = 100$ nm). The scale bars are 100 nm.

a monochromator. The monochromatic light was linearly polarized by a Glan–Thompson polarizer before reaching the device. Devices were mounted on a rotating stage, allowing measurements to be performed at different incident angles. Numerical simulations of the optical behavior of these structures were performed using rigorous coupled-wave analysis [17]. The dielectric properties of Ag and glass were modeled using the Lorentz–Drude model with material parameters from the published literature [18] that are known to correspond well to experimental measurements [19]. The refractive index of the spin-on glass (F215 from Filmtronics, Inc.) is assumed to be 1.35 and nondispersive. This value is very close to the refractive index of 1.38 specified by the manufacturer. We attribute the small difference to the low spin-on-glass annealing temperature (250°C) we employed to preserve the structure of the underlying Ag nanostructures, as the low-temperature annealing process may result in slightly reduced material density and refractive index.

## 3. RESULTS AND DISCUSSIONS

Previous work has shown that a single-layer plasmonic metasurface structure can provide low optical transmittance, due to the excitation of plasmonic resonances within individual metasurface elements, over a narrow range of wavelengths that remains fixed over angles of incidence ranging from 0° to approximately 60° off normal [20]. Figures 2(a) and 2(b) show optical transmittance measured for a single-layer metasurface structure consisting of 100 nm × 100 nm × 30 nm Ag patches (i.e., $W = 100$ nm) arranged in a square array with period $L = 200$ nm, as a function of wavelength, angle of incidence, and polarization of incident light. Figures 2(c) and 2(d) show the same quantities for a second single-layer metasurface structure consisting of a square array of 30 nm high Ag patches with $W = 170$ nm and $L = 300$ nm. As illustrated in the figures, the single-layer metasurfaces produce a minimum in transmittance coinciding approximately with the plasmonic resonance wavelengths in the individual Ag patches. For the metasurface with $W = 100$ nm and $L = 100$ nm [Figs. 2(a) and 2(b)], the transmittance is very weakly dependent on incident angle $\theta_i$ over the range $\theta_i = 0°$–$60°$. For the structure with $W = 170$ nm and $L = 300$ nm [Figs. 2(c) and 2(d)], the minimum in transmittance is shifted to slightly longer wavelengths due to the larger size of the individual Ag structures, and local peaks in transmittance appear at wavelengths near the plasmonic resonance wavelength due to Wood's anomaly and coupling to surface plasmon modes [20].

Figures 2(e)–2(h) show measured and numerically simulated optical transmittance spectra for an aligned ($S_x = S_y = 0$) multilayer structure consisting of a lower metasurface with $W_1 = 100$ nm and $L_1 = 200$ nm, an upper metasurface with $W_2 = 170$ nm and $L_2 = 300$ nm, and a spin-on-glass layer of thickness $D = 350$ nm separating the two metasurface layers. The measured and numerically simulated transmittance spectra are in excellent agreement, and demonstrate that the multilayer structure is able to produce a deep, broad minimum in transmittance—transmittance <1% over wavelengths from 550 to 650 nm—for both TE and TM polarizations and for angles of incidence $\theta_i$ from 0° to 30°. For angles of incidence from 0° to 20°, the transition to high optical transmittance (30%–50% or greater) occurs over a narrow wavelength range, ~30–50 nm, at both shorter and longer wavelengths. For incident angles of 30° or greater, a local maximum in transmittance begins to appear at ~650 nm, and becomes more prominent as $\theta_i$ increases. Simulated reflectance, transmittance, and absorption spectra as functions of wavelength, polarization, and incident angle indicate that reflectance and absorption within the low transmittance band is >75%, and ~20%, respectively, in the wavelength range of 600–700 nm.

Detailed numerical simulations provide insight into the origin of these behaviors, and into opportunities to engineer specific optical properties and realize designs that are robust to variations and imperfections that are most likely to arise in practical manufacturing processes. Figure 3 shows numerically simulated transmittance spectra under TE-polarized illumination for a multilayer structure containing two metasurfaces with $W_1 = 100$ nm, $L_1 = 200$ nm and $W_2 = 170$ nm, $L_2 = 300$ nm, separated by a spin-on-glass dielectric layer with thickness $D$ ranging from 40 to 600 nm. The layers are vertically aligned with $S_x = S_y = 0$. In Fig. 3(a), corresponding to normally incident illumination ($\theta_i = 0°$), we observe that there is a deep minimum in transmittance extending approximately from 550 to 650 nm that is present for all values of $D$. The wavelength boundaries of this region are modulated due to the presence of local peaks in transmittance, corresponding approximately to the solid curves in the figure, that occur at specific wavelengths for a given value of metasurface layer separation $D$. These transmittance peaks can be

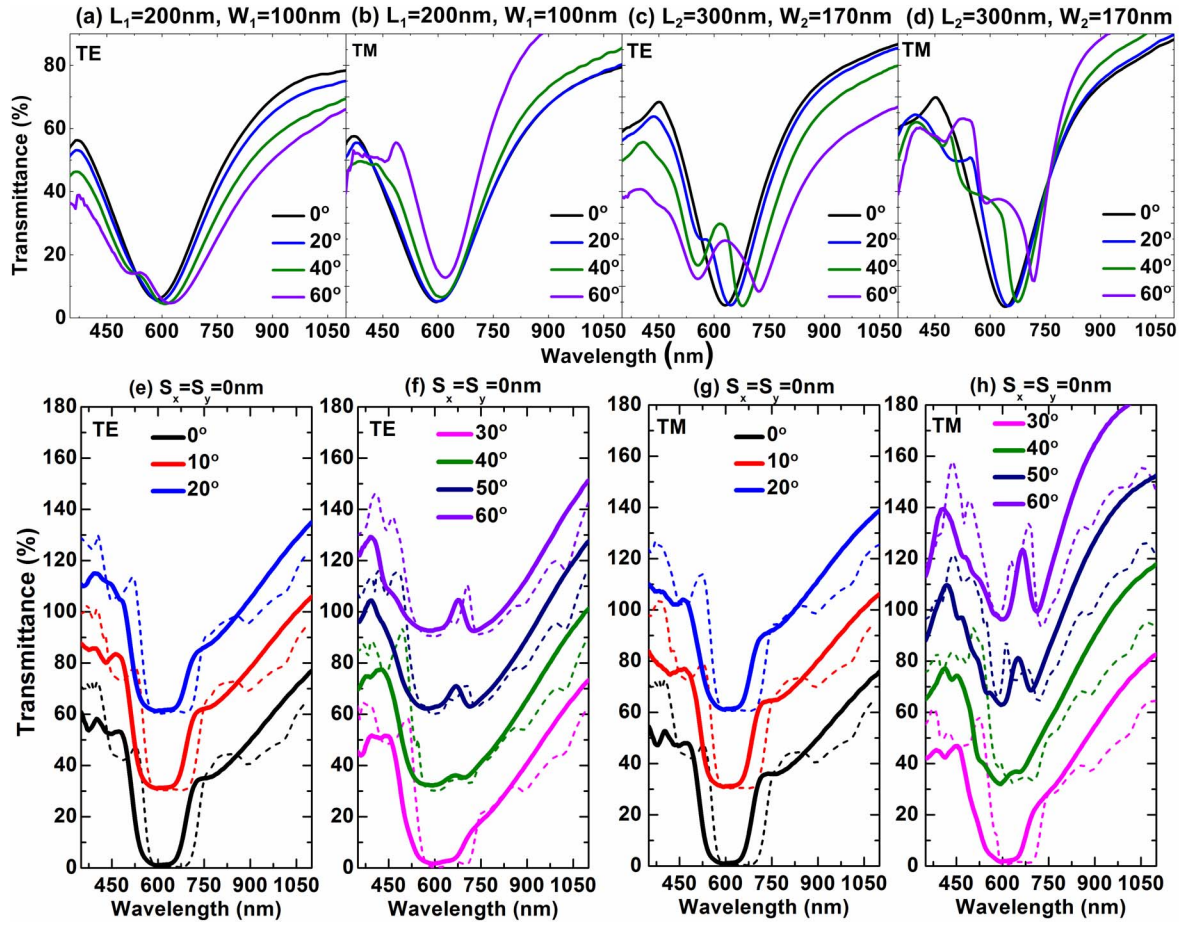


Fig. 2. (Color online) (a)–(d) Measured transmission spectra for $L_1 = 200$ nm, $W_1 = 100$ nm, and $L_2 = 300$ nm, $W_2 = 170$ nm single-layer metasurfaces under TE- and TM-polarized illumination, respectively. (e)–(h) Measured (solid curves) and simulated (dashed curves) transmission spectra for an aligned multilayer metasurface structure, $L_1 = 200$ nm, $W_1 = 100$ nm, $L_2 = 300$ nm, $W_2 = 170$ nm, $D = 350$ nm, and $S_x = S_y = 0$ under TE- and TM-polarized light, respectively. In parts (e)–(h), transmittance spectra at different incident angles have been offset vertically by 30% each for clarity.

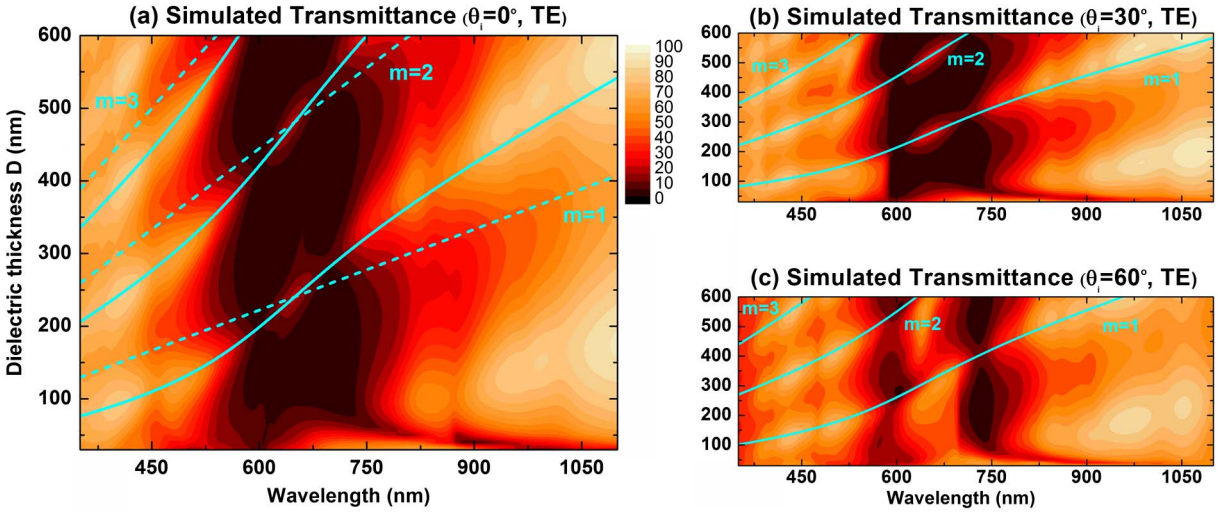


Fig. 3. (Color online) Simulated transmittance spectra, as a function of wavelength and dielectric layer thickness $D$ for a multilayer metasurface structure with $L_1 = 200$ nm, $W_1 = 100$ nm, $L_2 = 300$ nm, $W_2 = 170$ nm, and $S_x = S_y = 0$ for (a) $\theta_i = 0°$, (b) $\theta_i = 30°$, and (c) $\theta_i = 60°$ under TE-polarized light. The solid curves and dashed lines represent Fabry–Perot resonance wavelengths as given by Eq. (3) with and without, respectively, inclusion of the metasurface phase shift given by Eq. (2).

interpreted as arising from Fabry–Perot resonances created by the reflectance and transmittance properties of each metasurface, appropriately modified to account for the wavelength-dependent phase shift produced by each.

For conventional Fabry–Perot resonances, the wavelengths at which peaks in optical transmittance through a dielectric cavity of thickness $D$ would occur are given by

$$\lambda = \frac{2n_d}{m}D, \tag{1}$$

where $m$ is a positive integer corresponding to different cavity modes, $n_d$ is the refractive index of the dielectric material, and $\lambda$ is the wavelength in free space. The Fabry–Perot resonant wavelengths given by Eq. (1) with $n_d$ and $D$ taken to be the refractive index and thickness, respectively, of the spin-on glass, are indicated by the dashed lines in Fig. 3(a), revealing that this expression provides at best a very approximate estimate of the wavelengths at which such resonances occur in the multilayer metasurface structure. Much better agreement is obtained by accounting for the wavelength-dependent phase shift incurred upon interaction of light with the metasurface layers [21,22]. Specifically, the total wavelength-dependent phase shift produced by the two metasurfaces is given approximately by [22]

$$\phi(\lambda) \approx \tan^{-1}\left[\frac{2\pi c}{\gamma}\left(\frac{1}{\lambda}-\frac{1}{\lambda_r}\right)\right], \tag{2}$$

where $\gamma$ is a phenomenological damping constant obtained by fitting to transmittance or reflectance spectra, and $\lambda_r$ is the resonance wavelength in the multilayer metasurface structure. Given this phase shift, and following a recently developed approach for analysis of refraction in the presence of phase shifts [13], the Fabry–Perot resonance condition is modified from that given by Eq. (1) to become

$$\lambda = \frac{2\sqrt{n_d^2 - \sin^2\theta_i}}{m - \phi(\lambda)/\pi}D, \tag{3}$$

where $\phi(\lambda)$ is given by Eq. (2). The solid curves in Fig. 3(a) are the Fabry–Perot resonant wavelengths given by Eq. (3) with $n_d$ and $D$ taken to be the refractive index and thickness, respectively, of the spin-on glass, and with $\gamma = 3\times10^5$ s$^{-1}$ and $\lambda_r = 650$ nm determined by fitting to the computed transmittance spectra. We see that agreement between the Fabry–Perot resonant wavelengths computed using Eq. (3) and the transmittance peaks present in Fig. 3(a) is excellent. Figures 3(b) and 3(c) show numerically simulated transmittance spectra and Fabry–Perot resonant wavelengths computed using Eq. (3) for incident angles of 30° and 60°. Once again, excellent agreement is observed between the resonant wavelengths computed using Eq. (3) and the peaks observed in the numerically simulated transmittance spectra, providing clear evidence of the role of metasurface phase shifts in influencing optical transmittance in these structures.

The existence of transmittance peaks associated with phase-dependent Fabry–Perot resonances in multilayer metasurface structures offers an opportunity to optimize the wavelength sensitivity of transmittance via judicious selection of the thickness $D$ of the spin-on-glass layer. Figure 4(a) shows numerically simulated transmittance spectra for multilayer metasurface structures with $W_1 = 100$ nm, $L_1 = 200$ nm, $W_2 = 170$ nm, $L_2 = 300$ nm, $D = 250$–$450$ nm, and $S_x = S_y = 0$, for light incident with TE polarization. While a broad transmittance minimum is present over the entire range of values of $D$ shown, the positioning of the Fabry–Perot resonance transmission peaks at the edges of this transmittance minimum for $D \approx 300$–$380$ nm allows $D$ to be used a tuning parameter to produce (a) higher-contrast transitions with wavelength between low and high transmittance, and (b) moderate shifts in the center wavelength of the transmittance minimum. These trends are confirmed in experimental measurements. Figures 4(b) and 4(c) show measured transmittance spectra for multilayer metasurface structures with $W_1 = 100$ nm, $L_1 = 200$ nm, $W_2 = 170$ nm, $L_2 = 300$ nm, and $D = 300$, 350, and 380 nm. The layers are vertically aligned, with $S_x = S_y = 0$. Measurements for angles of incidence of 0° and 30°, and for both TE and TM polarization, are shown. The positioning of the Fabry–Perot transmittance peak at ~700 nm for $D = 350$ nm and $D = 380$ nm leads to a substantial increase in contrast between the low- and high-transmittance regions of the measured spectra on either side of the transmittance peak. Furthermore, the shift in position of the Fabry–Perot transmittance peak between $D = 350$ nm and $D = 380$ nm allows the center wavelength of the transmittance minimum to be shifted by ~50 nm while maintaining a fixed bandwidth of ~100 nm.

Vertical alignment of nanoscale features is often a key concern in design and fabrication of multilayer or three-dimensional nanostructures. For applications requiring

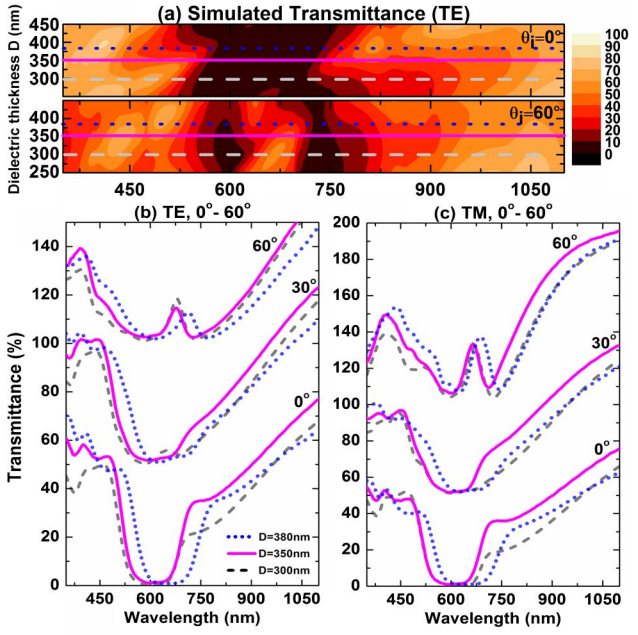


Fig. 4. (Color online) (a) Simulated transmittance spectra for $\theta_i = 0°$ and $\theta_i = 60°$ under TE polarization. Dashed, solid, and dotted lines correspond to dielectric layer thicknesses $D = 300$, 350, and 380 nm, respectively. (b),(c) Measured transmittance spectra for multilayer metasurface structures with $L_1 = 200$ nm, $W_1 = 100$ nm, $L_2 = 300$ nm, $W_2 = 170$ nm, $S_x = S_y = 0$, and $D = 300$, 350, and 380 nm, following the same plot scheme as in (a), under TE or TM polarization, respectively. In parts (b) and (c), transmittance spectra at different incident angles have been offset vertically by 50% each for clarity.

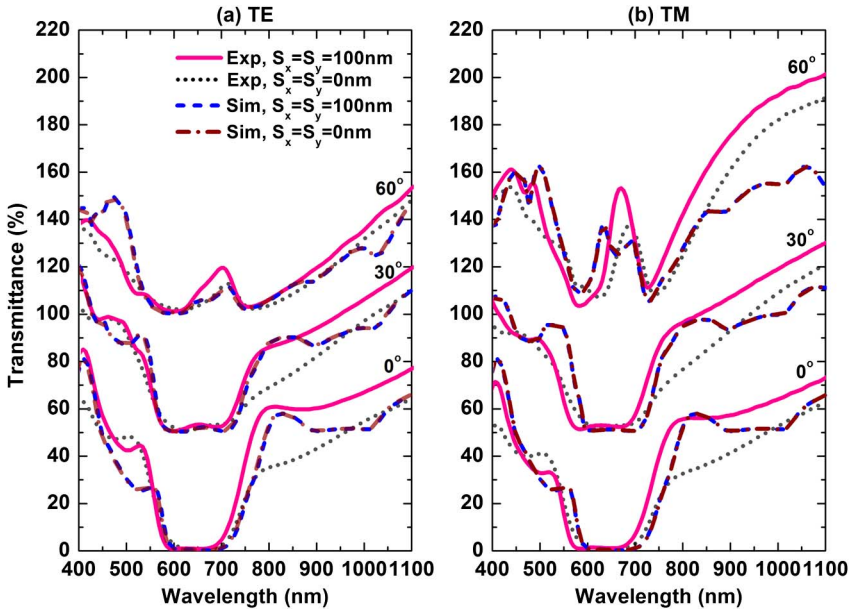


Fig. 5. (Color online) Measured and simulated transmission spectra for a multilayer metasurface structure with $L_1 = 200$ nm, $W_1 = 100$ nm, $L_2 = 300$ nm, $W_2 = 170$ nm, $D = 380$ nm, and $S_x = S_y = 100$ nm or $S_x = S_y = 0$ nm for different $\theta_i$ under (a) TE or (b) TM polarization. Transmittance spectra at different incident angles have been offset vertically by 50% each for clarity.

fabrication at low cost or over large areas, it would be highly desirable to design structures whose performance characteristics are robust to variations in vertical alignment. For the multilayer metasurface structures considered here, the transmittance and reflectance properties depend primarily on plasmonic resonant phenomena in each individual metallic nanostructure. Interactions between these individual elements in the vertical direction do not play a significant role since the vertical distance between the two layers, $D$, is much larger than the extent of the electromagnetic near fields associated with these plasmonic resonances. The optical properties of the multilayer metasurface structures presented here are therefore extremely robust to even large variations in vertical alignment, i.e., values of $S_x$ and $S_y$ that are substantial fractions of $W$ or $L$ for the individual metasurface layers; for sufficiently small values of $D$, these interactions would become significant and greater sensitivity to vertical misalignment would be expected. Figure 5 shows numerically simulated measured optical transmittance spectra for a multilayer metasurface structure with $W_1 = 100$ nm, $L_1 = 200$ nm, $W_2 = 170$ nm, $L_2 = 300$ nm, $D = 380$ nm, and $S_x = S_y = 100$ nm or $S_x = S_y = 0$. We note that this is the maximum translational misalignment, relative to $S_x = S_y = 0$, that can occur for this structure. Despite this misalignment, the measured optical transmittance spectra are nearly identical to those of the corresponding structure with $S_x = S_y = 0$ shown in Figs. 5(a) and 5(b) for the transmittance, and with minor differences in the longer wavelengths due to different Fabry–Perot resonant wavelengths introduced by fabrication imperfections of Ag and spin-on glass.

## 4. CONCLUSIONS

In summary, we have designed, experimentally demonstrated, and analyzed both numerically and analytically a series of multilayer plasmonic metasurface structures that provide wide-angle, wavelength-selective, polarization-independent optical transmittance and reflectance with performance that is robust to even severe vertical misalignment between individual plasmonic metasurface arrays constituting the complete multilayer structure. These characteristics are shown to be a consequence of high reflectivity associated with plasmonic resonances in each metasurface layer, phase shifts induced by interaction of light with the metasurfaces, and phase-dependent Fabry–Perot resonances associated with the multilayer stack. The insensitivity of the wavelength-dependent optical reflectance and transmittance to polarization and angle of incidence suggest potential use of these types of structures for a broad range of applications. Robustness to severe vertical misalignment between individual layers in a multilayer structure suggests that these structures can be highly amenable to low-cost, high-throughput fabrication processes.

## ACKNOWLEDGMENTS

Part of this work was supported by the National Science Foundation (ECCS-1128682 and ECCS-1120823) and the Judson S. Swearingen Regents Chair in Engineering at the University of Texas at Austin. P. C. Li would like to thank L. Zhu, C. O. McPheeters, and Y. Zhao for discussions on details of fabrications and simulations.

## REFERENCES

1. M. Decker, M. Ruther, C. E. Kriegler, J. Zhou, C. M. Soukoulis, S. Linden, and M. Wegener, "Strong optical activity from twisted-cross photonic metamaterials," Opt. Lett. **34**, 2501–2503 (2009).
2. D. Dregely, R. Taubert, J. Dorfmuller, R. Vogelgesang, K. Kern, and H. Giessen, "3D optical Yagi-Uda nanoantenna array," Nat. Commun. **2**, 267 (2011).
3. J. Ye, F. Wen, H. Sobhani, J. B. Lassiter, P. V. Dorpe, P. Nordlander, and N. J. Halas, "Plasmonic nanoclusters: near field properties of the Fano resonance interrogated with SERS," Nano Lett. **12**, 1660–1667 (2012).
4. C. Wu, A. B. Khanikaev, R. Adato, N. Arju, A. A. Yanik, H. Altug, and G. Shvets, "Fano-resonant asymmetric metamaterials for

ultrasensitive spectroscopy and identification of molecular monolayers," Nat. Mater. **11**, 69–75 (2012).
5. Y. Cui, K. H. Fung, J. Xu, H. Ma, Y. Jin, S. He, and N. X. Fang, "Ultrabroadband light absorption by a sawtooth anisotropic metamaterial slab," Nano Lett. **12**, 1443–1447 (2012).
6. Z. H. Jiang, S. Yun, F. Toor, D. H. Werner, and T. S. Mayer, "Conformal dual-band near-perfectly absorbing mid-infrared metamaterial coating," ACS Nano **5**, 4641–4647 (2011).
7. X. Liu, T. Starr, A. F. Starr, and W. J. Padilla, "Infrared spatial and frequency selective metamaterial with near-unity absorbance," Phys. Rev. Lett. **104**, 207403 (2010).
8. W. Cai, U. K. Chettiar, H.-K. Yuan, V. C. de Silva, A. V. Kildishev, V. P. Drachev, and V. M. Shalaev, "Metamagnetics with rainbow colors," Opt. Express **15**, 3333–3341 (2007).
9. J. Valentine, S. Zhang, T. Zentgraf, E. Ulin-Avila, D. A. Genov, G. Bartal, and X. Zhang, "Three-dimensional optical metamaterial with a negative refractive index," Nature **455**, 376–379 (2008).
10. N. Liu, H. Guo, L. Fu, S. Kaiser, H. Schweizer, and H. Giessen, "Three-dimensional photonic metamaterials at optical frequencies," Nat. Mater. **7**, 31–37 (2008).
11. N. Liu, M. Hentschel, T. Weiss, A. P. Alivisatos, and H. Giessen, "Three-dimensional plasmon rulers," Science **332**, 1407–1410 (2011).
12. S. H. Lim, W. Mar, P. Matheu, D. Derkacs, and E. T. Yu, "Photocurrent spectroscopy of optical absorption enhancement in silicon photodiodes via scattering from surface plasmon polaritons in gold nanoparticles," J. Appl. Phys. **101**, 104309–104307 (2007).
13. N. Yu, P. Genevet, M. A. Kats, F. Aieta, J.-P. Tetienne, F. Capasso, and Z. Gaburro, "Light propagation with phase discontinuities: generalized laws of reflection and refraction," Science **334** 333–337 (2011).
14. E. F. Kuester, M. A. Mohamed, M. Piket-May, and C. L. Holloway, "Averaged transition conditions for electromagnetic fields at a metafilm," IEEE Trans. Antennas Propag. **51**, 2641–2651 (2003).
15. J. A. Gordon, C. L. Holloway, and A. Dienstfrey, "A physical explanation of angle-independent reflection and transmission properties of metafilms/metasurfaces," IEEE Antennas Wirel. Propag. Lett. **8**, 1127–1130 (2009).
16. H. A. Macleod, *Thin-Film Optical Filter* (CRC, 2010).
17. L. Li, "New formulation of the Fourier modal method for crossed surface-relief gratings," J. Opt. Soc. Am. A **14**, 2758–2767 (1997).
18. A. D. Rakic, A. B. Djuric, J. M. Elazar, and M. L. Majewski, "Optical properties of metallic films for vertical-cavity optoelectronic devices," Appl. Opt. **37**, 5271–5283 (1998).
19. E. D. Palik, *Handbook of Optical Constants of Solids* (Academic, 1991).
20. P.-C. Li, Y. Zhao, A. Alu, and E. T. Yu, "Experimental realization and modeling of a subwavelength frequency-selective plasmonic metasurface," Appl. Phys. Lett. **99**, 221106–221103 (2011).
21. A. Alu and N. Engheta, *Optical Wave Interaction with Two-Dimensional Arrays of Plasmonic Nanoparticles* (Cambridge University, 2011).
22. R. Taubert, R. Ameling, T. Weiss, A. Christ, and H. Giessen, "From near-field to far-field coupling in the third dimension: retarded interaction of particle plasmons," Nano Lett. **11**, 4421–4424 (2011).